



VICTORIA UNIVERSITY
MELBOURNE AUSTRALIA

ANFIS-based droop control of an AC microgrid system: considering intake of water treatment plant

This is the Published version of the following publication

Rohmingtuanga, C, Datta, Subir, Sinha, Nidul, Ustun, Taha Selim and Kalam, Akhtar (2022) ANFIS-based droop control of an AC microgrid system: considering intake of water treatment plant. *Energies*, 15 (19). ISSN 1996-1073

The publisher's official version can be found at
<https://www.mdpi.com/1996-1073/15/19/7442>

Note that access to this version may require subscription.

Downloaded from VU Research Repository <https://vuir.vu.edu.au/46817/>

Article

ANFIS-Based Droop Control of an AC Microgrid System: Considering Intake of Water Treatment Plant

C. Rohmingluanga ^{1,*}, Subir Datta ¹, Nidul Sinha ², Taha Selim Ustun ^{3,*} and Akhtar Kalam ^{4,*}¹ Department of Electrical Engineering, Mizoram University, Aizawl 796004, Mizoram, India² Department of Electrical Engineering, NIT Silchar, Silchar 788010, Assam, India³ Fukushima Renewable Energy Institute, AIST (FREA), Koriyama 963-0298, Japan⁴ College of Engineering and Science, Victoria University, Footscray, VIC 3011, Australia

* Correspondence: crotea.research@gmail.com (C.R.); selim.ustun@aist.go.jp (T.S.U.); akhtar.kalam@vu.edu.au (A.K.)

Abstract: Provision of an efficient water supply system (WSS) is one of the top priorities of all municipals to ascertain adequate water supply to the city. Intake is the lifeline of the water supply system and largely effects the overall plant efficiency. The required power supply is generally fed from the main grid, and a diesel generator is commonly used as a power backup source. This results in high pumping cost as well as high operational cost. Moreover, due to operation of motor pumps and other auxiliary loads, frequent maintenance is required. Therefore, to avoid various challenges and to efficiently operate the intake system, microgrid concept has been introduced in this paper. Various distributed generations (DGs) such as solar photovoltaic (PV), interior permanent magnet machine (IPM) wind turbine generator and Battery energy storage system (BESS) are incorporated in the microgrid system. Additionally, a new approach based on adaptive neuro-fuzzy inference system (ANFIS) is proposed, where P-f and Q-V droop is considered while training the ANFIS data; after successful training, the microgrid voltage and frequency are controlled as per system requirement. Simulation of the microgrid system shows good results and comparison with the generalized droop control (GDC) method is done using MATLAB/Simulink software.

Keywords: microgrid; intake; photovoltaic (PV); interior (or buried) permanent magnet machines (IPM)-based wind turbine generator; battery energy storage system (BESS); adaptive neuro-fuzzy inference system (ANFIS); droop control



Citation: Rohmingluanga, C.; Datta, S.; Sinha, N.; Ustun, T.S.; Kalam, A. ANFIS-Based Droop Control of an AC Microgrid System: Considering Intake of Water Treatment Plant. *Energies* **2022**, *15*, 7442. <https://doi.org/10.3390/en15197442>

Academic Editors: Sidun Fang, Liang Liang and Yun Yang

Received: 8 September 2022

Accepted: 8 October 2022

Published: 10 October 2022

Publisher's Note: MDPI stays neutral with regard to jurisdictional claims in published maps and institutional affiliations.



Copyright: © 2022 by the authors. Licensee MDPI, Basel, Switzerland. This article is an open access article distributed under the terms and conditions of the Creative Commons Attribution (CC BY) license (<https://creativecommons.org/licenses/by/4.0/>).

1. Introduction

As water is the main source of survival for every living being on Earth, conservation of water sources and improvement of the pumping and treatment is very important due to climate change and increase of pollutions in the environment. Additionally, due to huge consumption of fossil fuel, i.e., coal, natural gas and oil, energy consumption cost has been increasing day by day, and it is a very important factor to be considered while operating public water treatment plant and industries. Generally, a water supply system consists of raw water pumping station (also called as Intake), water treatment plant (clear water pumping station) and intermediate pumping stations (booster) and main Reservoir. The required raw power supply of each pumping stations is drawn from the grid through distribution companies or power and electricity department. Additionally, the power requirement of each pumping station depends on the plant design and capacity of each pump design.

The single line diagram (SLD) of a typical Intake is shown in Figure 1. Unlike other industries/plant the power requirement for the plant is drawn under high tension (HT) category (also considered as a bulk-consumers) and further stepped down to low tension (LT) for auxiliary loads, as shown in the figure, apart from the main power supply, a HT diesel generator is provided for standby power supply, and the step-down power transformer feeds various auxiliary loads, which could be around 5–20% of the total loads.

As public water treatment plant falls under the category of bulk consumers, the running cost as well as the energy cost becomes one of the Government and municipal burden every year. Additionally, operational cost of a diesel generator (DG) set alone contributes huge financial burden, and it is being used by almost all of the water treatment plant so as to meet energy demand during power failure. Not only that, the production of pollutants (particularly CO₂ gas) into the atmosphere harms the environment in many ways. Therefore, Considering the importance and ever-ending demand of reliable public water supply, sustainable treatment as well as sustainable power supply becomes very important so as to improve the treatment as well as reduce the burden of every municipals.

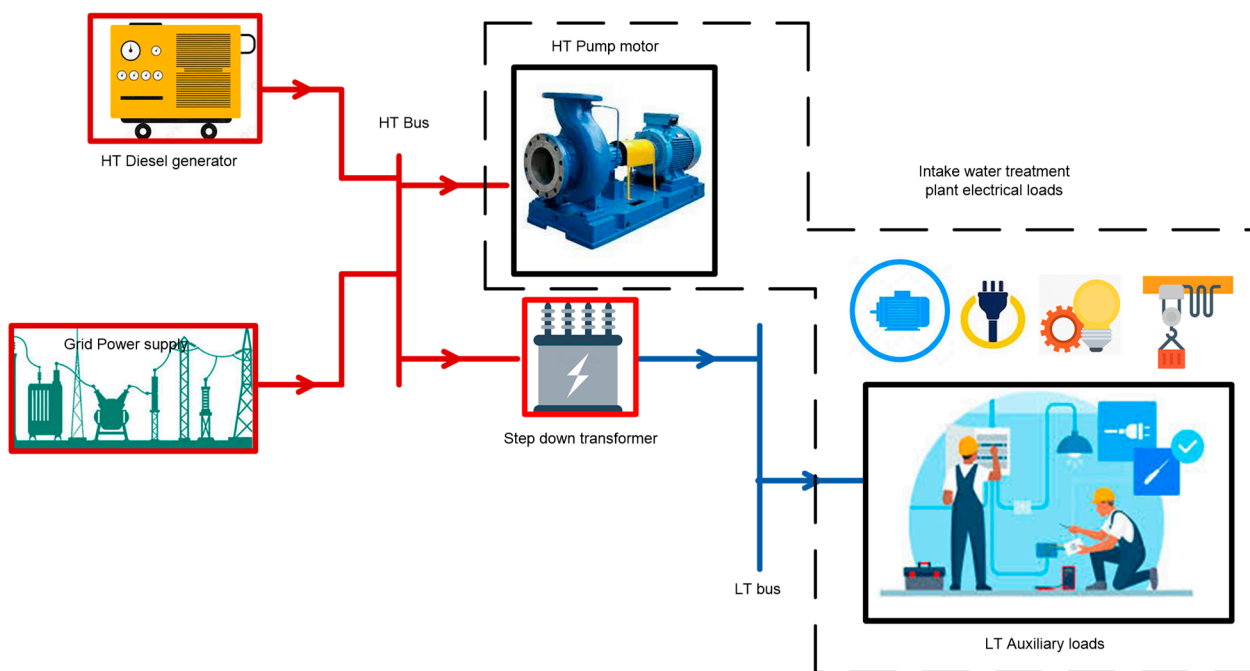


Figure 1. SLD of typical Intake system.

The introduction of distributed energy resources (DER) commonly referred as distributed generation (DG) plays an important role in many power sector applications and could also be applied to the aforesaid problems, especially being faced with a water supply system. Due to the decentralized nature and flexibility, RES becomes more and more popular to overcome the ever-increasing energy demand and is being used in many applications to provide various auxiliary power demand. Moreover, DER offers a wide range of applications and are linked and incorporated with the main grid using control panels and power electronic devices such as converters. In this connection, introduction of microgrid concept in the aforesaid applications can be a game changer for solving various issues and problems encountered in the fields of power sectors.

A microgrid can be defined as an independent energy system (such as university campus, industrial complex, military complex, treatment plants and neighborhood, etc.) consisting of various loads and one or more distributed energy source such as solar panels, wind turbines, battery energy storage system, generators, etc. Microgrid normally operates in synchronous with the grid (grid connected mode) and in case of fault occurrence on the line/grid side, microgrid isolates itself from the main grid and activates the islanded mode of operation, so as to provide uninterrupted power supply to the system. There are different types of control techniques available in grid-connected and in islanded modes, one of the challenges being faced in the microgrid environment is to maintain the system frequency and control the voltage while ensuring the system stability. In grid-connected mode of operation, the basic primary focus is energy management. On the other hand, in an islanded mode of operation, the primary objective becomes control of the frequency as

well as the voltage while satisfying the energy demand. Synchronous machine is generally provided to balance supply and demand of power in many system operations. However, if the microgrid system do not contain synchronous machine, inverter alone plays a very important role in providing frequency and voltage control especially in islanded mode of operation [1,2]. In short, Active Power (P) as well as Reactive Power (Q) control strategy is being used in the grid-connected mode, and quickly changes its control to voltage frequency control (V/f), when an islanded mode of operation is activated. Additionally, the centralized control architecture is widely used in traditional power networks mainly at the generating station. Whereas, under DER/DG applications, decentralized control architectures are generally applied and used [3,4].

Apart from the above case, the microgrid line impedance of different voltage level plays a very important role in considering droop control, generally, in a low voltage (LV) based microgrid system. the lines are normally assumed to be more resistive and thereby considered a relation between (P-V), active power (P) & voltage (V) similarly, (Q-f), reactive power (Q) & frequency (f) relations is considered. Therefore, P-V and Q-f droop combinations and its relations are considered for control of the microgrid voltage and frequency [5,6]. Moreover, in a medium voltage (MV) microgrid system, the lines are assumed to be more inductive and hence (P-f), active power (P) & frequency (f) relations is considered similarly, (Q-V), reactive power(Q) & voltage (V) relation is considered. Therefore, improved droop methods, i.e., P-f and Q-V droops and its variants are used for controlling the frequency and voltage [7–9]. In line with this, intake of the water treatment plant could be considered as a combination of low voltage and medium voltage loads acting as a separate unit, therefore, resistance as well as the inductance are considered in the line. In this paper the respective P-f and Q-V droop and is considered for controlling the frequency and voltage while considering intake microgrid system [10,11].

Apart from the above, some study shows that due to the periodic and fluctuating nature of renewable sources such as wind and solar, the power producing capacity of such DGs is also varying and periodic. Therefore, monitoring and compensation of the reactive power is very important to avoid problems such as voltage change, transient stability and voltage collapse. Figure 2 shows different classification of MG stability and, stability in microgrid are categorized into two phenomena such as short-term phenomena (may last up to only a few seconds) and long-term phenomena. Other stability issues more than the short-term phenomena timeframe are categorized as long-term stability. As per requirement, different control methods are available to prevent instability [12,13]. In order to solve various problems, including stability issues related to microgrid systems, as mentioned earlier, several efforts have been proposed in various papers. Mostly, microgrid systems are integrated with various renewable energy sources and power electronic devices; improved energy storage elements have been incorporated for compensating energy deviations.

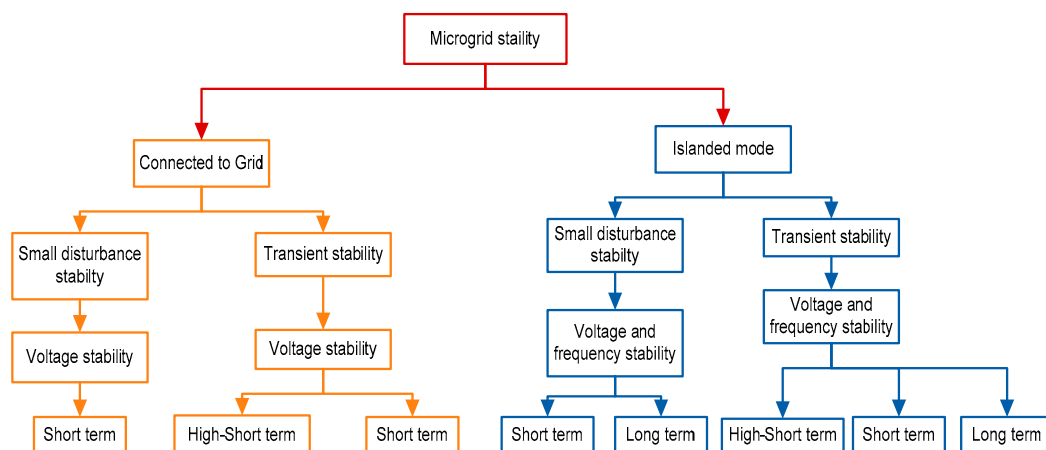


Figure 2. Microgrid stability.

The droop control technique is commonly used to regulate the voltage and frequency for achieving power sharing in the microgrid system and most of the islanded microgrids are operated under droop control techniques. The generalized droop control technique performs well only under grid connected mode, this is due to the fact that generalized droop control relies on the inverter output impedance and impedance of the line between DGs and loads. However, it is difficult to chalk out the accurate line impedance value between the DGs and the corresponding load when the number of DG units are more [14,15]. Additionally, droop control requires further development and possesses drawbacks, such as the high droop coefficients, which may cause deviations in voltage and frequency, and this can compromise the grid stability. In addition, due to requirement of complex transformation of the microgrid parameters, implementation of droop control in microgrid is difficult [16,17]. Therefore, in order to avoid the aforesaid issues and to remove dependency on line parameters, different intelligent methods such as artificial neural network (ANN), adaptive neuro fuzzy inference system (ANFIS) and Fuzzy logic, etc. are being used in references [18,19].

Recent studies proposed various control schemes for power quality improvement in grid connected mode of operation, whereas voltage and frequency regulation in islanded mode of operation. Furthermore, introduction of intelligent based frequency control techniques has been immersed in many scenarios which seems to improve the system response compared to conventional methods. Additionally, application of ANN and fuzzy logic controller (FLC) based frequency regulation in an islanded microgrid is seen in [20,21]. Many literatures suggested use of a storage elements such as batteries, electric vehicles, fuel cells, capacitors, flywheel storage, etc. to regulate the frequency [22,23]. Similarly, this paper has been formulated based on battery storage-based frequency regulation considering intake (public water supply) microgrid system with permanent magnet-based wind turbine and solar photovoltaic system. Additionally, latest intelligent techniques such as Artificial Neural Networks (ANNs), Fuzzy Logic Control (FLC), and Adaptive Neuro Fuzzy Inference (ANFIS) are being used in many papers [24,25]. However, application of microgrid system focusing on intake of the water supply system is not yet to be seen in literature. As intake consist mainly motor loads, the focus of the paper is to resolve the problem of frequency deviations in the microgrid system, this paper proposes droop control of a microgrid using Adaptive Neuro Fuzzy Inference System (ANFIS) technique.

The main objectives of this paper are:

1. To consider intake of water treatment plant as a microgrid system;
2. To implement DGs on the microgrid system;
3. To implement droop control and apply the Adaptive Neuro Fuzzy Inference ANFIS technique;
4. To analyze and compare the result with generalized droop control (GDC) method.

The rest of the paper is organized as follows: Intake microgrid configuration and modelling is discussed in Section 2, and Control unit Diagram is discussed in Section 3, in Section 4 ANFIS-based Droop Control Approach is discussed, follows by Results and Discussion in Section 5, and finally conclusions are addressed in Section 6.

2. Intake Microgrid Configuration and Modeling (Topology)

One of the main objectives of a Microgrid system is to maintain equilibrium power flow between demand and supply within the system. In islanded mode of operation, the equilibrium in power flow between supply and demand is generally accomplished by performing load shedding or by adjusting the amount of power generation. Considering Intake microgrid system, various DG units viz. non-renewable (e.g., natural gas, diesel, thermal, nuclear, etc.) or renewable energy sources (e.g., wind, solar, hydro, etc.) can be utilized so as to improves the system performance [26,27]. Particularly, wind energy contributes less harmonics in the system compare to other renewable energy sources. However, in standalone system, the system is prone to frequency fluctuations due to its low inertia.

Figure 3 represents the configuration of the proposed intake microgrid system. The intake system has been considered as a microgrid system comprising of HT loads and auxiliary LT loads. In grid connected mode, the power supply from the grid is further stepped down to feed the mentioned various HT and LT loads. The general configuration of the intake microgrid system consist of two voltage levels. First, HT power system, comprises a parallel combination of HT (such as 11 kV) grid and HT Diesel generator, providing power supply to the HT load such as pumps. Second, LT power voltage level has been provided through step down power transformer for feeding various LT loads such as compound lighting, quarters and office, etc. In the LT side of the microgrid, implementation of various DGs such as PV system, battery energy storage system (BESS) and permanent magnet-based wind turbine generator such as interior (or buried) permanent magnet machines (IPM) are also provided as a backup power source, as shown in the figure. These DGs are interlinked with a boost converter (DC to DC) through voltage source converter. Similarly, the BESS is coupled to the converter (DC side) using bidirectional DC to DC converter. From the PV array, the boost converter (DC to DC) extracts the maximum available power to compensate for the load using maximum power point tracking (MPPT). On the other hand, the bidirectional converter provides charging and discharging of the battery. Additionally, BESS keeps the dc-link voltage of the converter constant while providing required power supply irrespective of change in PV power output. IPM based wind turbine generator is linked to the DC side of the converter via boost converter (DC to DC). The converters are further connected to the DC-AC converter through DC link. The output of the converter is fed to the LT bus through LC filter and a coupling inductor. Various LT loads are connected at LT bus or point of common coupling (PCC).

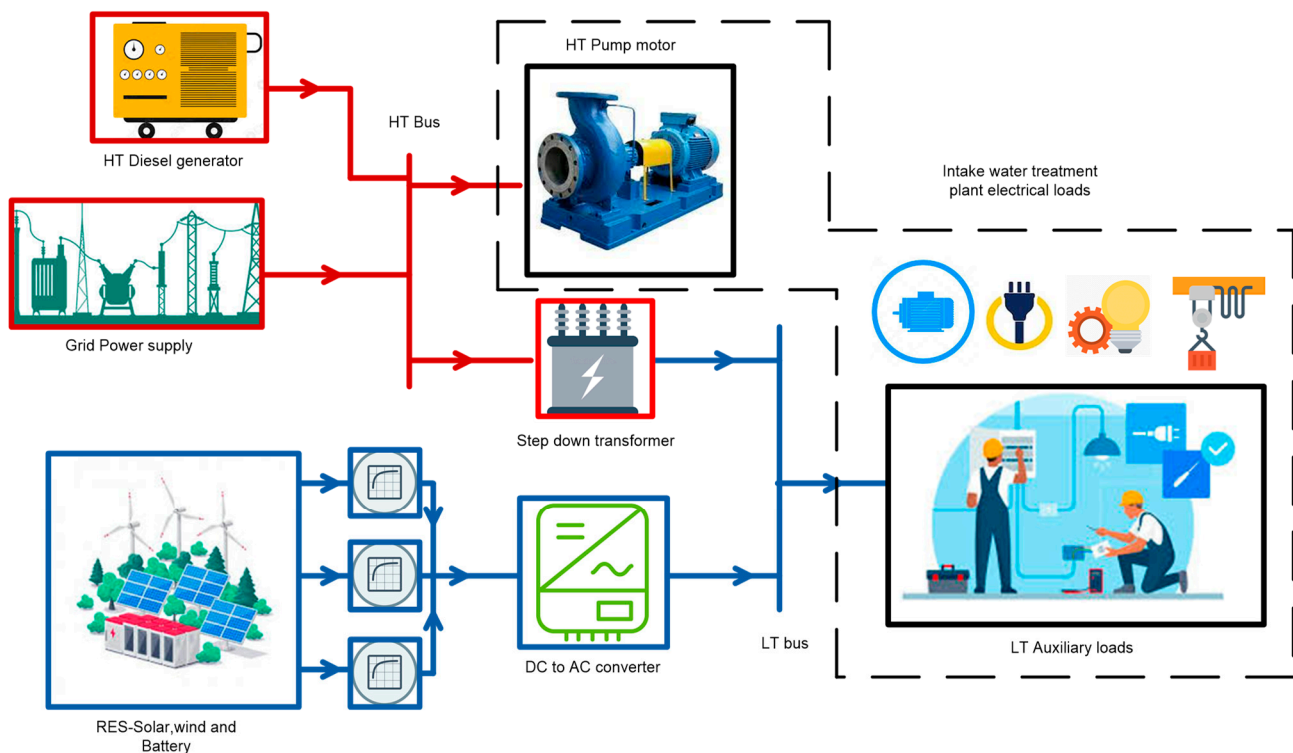


Figure 3. Single line configuration of the proposed microgrid system.

As the proposed microgrid system contains HT and LT combinations, Diesel engine generator alone is sufficient enough for the whole power back up, i.e., for HT load as well as LT load. However, due to high operational cost and maintenance cost, Diesel generator has been considered only for HT load. Therefore, in this paper various DGs are proposed for LT side only and the control strategy of the system has been considered only for the

LT side of the microgrid system. Tables 1 and 2 show details of the various loads and DGs connected to the intake microgrid system.

Table 1. Various loads of the microgrid system.

Sl. No.	Load	Power	Unit
1	Raw water pump 1	350	kW
2	Raw water pump 2	350	kW
3	Indoor & outdoor lighting	2.5	kW
4	Sludge pump	2.8	kW
5	Auxiliary load	1.9	kW

Table 2. Various DGs of the microgrid system.

Sl. No.	Source	Value	Unit
1	Solar	2.5	kW
2	Battery	1.5	kW
3	Wind	1	kW
4	HT Diesel generator	1000	kVA

As the microgrid system operates in grid connected mode and islanded mode, the proposed intake microgrid system has been designed and considered to operate in both modes of operation. Table 3 shows the operation of microgrid in grid connected and islanded mode of operation. In grid connected mode, various load such as Motor load, pumps and Light load, etc. are operated as per system requirement so as to pump maximum water from the river. The main power supply from the grid supplies power to the system in full, and BESS harvested the energy generated from the PV and Wind energy sources while providing the required power supply to the system. Additionally, as per requirement extra energy generated from the RES can be used to compensate power cost from the grid. In islanded mode of operation, the intake system gets isolated from the main grid and governs its own power flow, i.e., Diesel generator and RESs feeds the system in full while isolated from the main grid supply. Additionally, various converter plays a very important role in control and energy conversion. Management of power flow and optimization of stability in the system has been achieved by performing droop control in both the operating conditions.

Table 3. Operation timeline of microgrid in grid connected and islanded mode.

Sl. No.	Grid Connected (0–0.5)	Islanded (0.5–1)	Load (HT/LT)	Operation Time (s)
1	On	On	Raw water pump 1	0–1
2	On	On	Raw water pump 2	0–1
3	Off	On	Indoor & outdoor lighting	0–0.6
4	Off	On	Sludge pump	0.2–0.8
5	Off	On	Auxiliary load	0.4–0.9

2.1. Modeling and Control of PV with Battery System

Several renewable energy generation technologies have been utilized and practiced nowadays, out of these, solar photo voltaic system is one of the most important renewable energy generation sources and is being commonly used in many countries. The Solar PV system has various advantages such as pollution free, less maintenance cost and no fuel costs, etc., it is easy to install, and it plays a very important role in reduction of greenhouse gases and contributes positive impact in many environmental concerns. Therefore, it is ideal and a very good alternate source, when it comes to the topic of replacement of fossil fuel energy generations [28,29].

Under grid connected mode of operation, the main concern regarding control is power sharing between load and source, however in islanded or stand-alone mode of

operation, the power sharing as well as voltage and frequency control becomes very important, in order to achieve this proper design and calculation of the microgrid system is required. Additionally, the dynamics of the loads and the power sources must be properly considered [30,31]. In islanded mode of operation, the PV system may not always follow the maximum power point in order to balance the sources and loads. Therefore, in order to satisfy the load requirements viz. linear and nonlinear loads, provision of additional energy source like a battery energy storage system (BESS) is required to optimize the operation of Solar PV system. In this paper, combination of PV system and battery energy sources is considered to obtain maximum power and control of DC link voltage is achieved by implementing electronic converters.

Figure 4 shows the schematic diagram of the Solar PV with BESS system. Here, solar PV and BESS are connected to DC link capacitor and further connects to the three-phase inverter (DC-AC). A DC to DC boost converter is used to boost the solar output voltage magnitude as per system requirement, and hence, it is basically used to drive the solar PV output power. Similarly, A bi-directional DC-to-DC converter is connected to the battery energy storage system, the converter alters the course of switching by charging or discharging the battery while achieving the DC link voltage. The three-phase inverter is used to convert DC voltage to AC voltage and controls the load voltage magnitude. In this paper, various loads analogous to intake LT loads are considered and implemented in MATLAB Simulink environment.

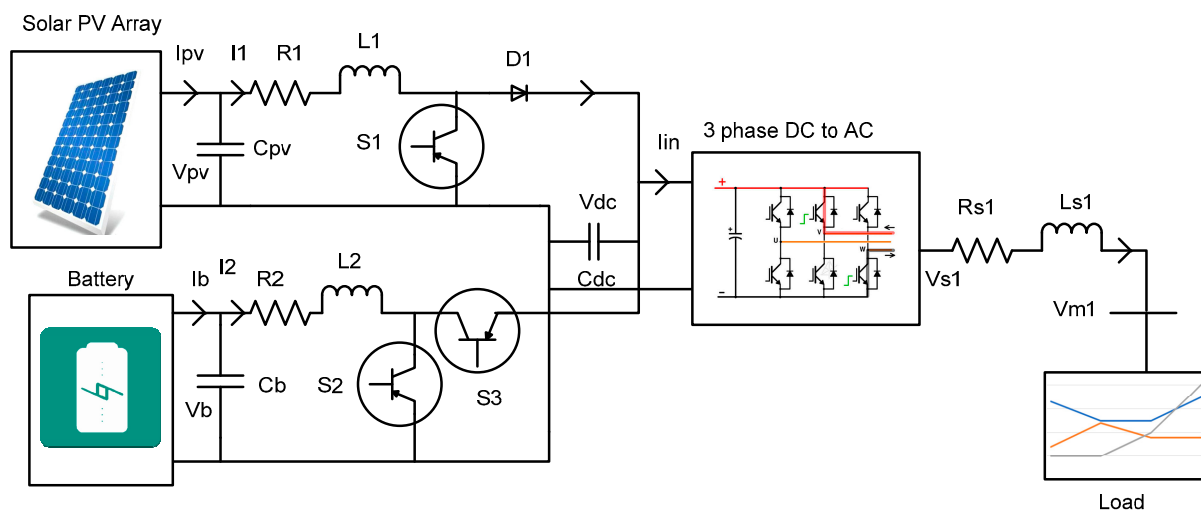


Figure 4. Schematic diagram of PV with Battery inverter system.

2.1.1. Solar Photo Voltaic (SPV) System

The designed parameters of the solar PV system are shown in Table 4, the solar PV system equation of the nonlinear model relating to the PV current and the terminal voltage is defined in the following equations

$$I_{pv} = n_p I_{ph} - n_p I_{rs} \left[\exp \left(\frac{q}{k\theta A} \frac{V_{pv}}{n_s} \right) - 1 \right] \quad (1)$$

$$I_{ph} = [I_{scr} + k_\theta (\theta - \theta_r)] \frac{S}{100} \quad (2)$$

where I_{rs} and θ represents the reverse saturation current and the temperature of $p - n$ junction. A is the ideality factor I_{scr} is the short-circuit current of a single PV cell and S is solar irradiation level, n_s and n_p are the series and parallel number of PV cells in a string, q ($=1.602 \times 10^{-19}$ C) and k ($=1.38 \times 10^{-23}$ J/K) are the unit electric charge and Boltzmann's constant respectively, also, θ_r is the cell temperature reference and k_θ is the temperature coefficient [32,33].

Table 4. Parameters of the PV system.

Parameters	Values	Parameters	Values
θ	289 °k	n_p	249
q	1.602×10^{-19} C	I_{src}	8.12A
S	1.2	θ_r	300 °k
I_{rs}	1.8×10^{-7}	n_s	238
A	1.692	k_θ	0.0014
K	1.38×10^{-23} J/K		

Similarly, equations for Boost Converter and the PV System can be defined as follows
When S_1 is ON ($S_1 = 1$)

$$C_{pv} p V_{pv} = I_{pv} - I_1 \quad (3)$$

$$V_{pv} = L_1 p I_1 + R_1 I_1 \quad (4)$$

When, S_1 is Off ($D_1 = 1$)

$$C_{pv} p V_{pv} = I_{pv} - I_1 \quad (5)$$

$$V_{pv} = L_1 p I_1 + R_1 I_1 + V_{dc} \quad (6)$$

Therefore, from the above equations ($D_1 = 1 - S_1$)

$$C_{pv} p V_{pv} = I_{pv} - I_1 \quad (7)$$

$$V_{pv} = L_1 p I_1 + R_1 I_1 + (1 - S_1) V_{dc} \quad (8)$$

2.1.2. Battery Energy Storage System (BESS)

Battery have been widely used in many applications nowadays, and the commonly used grid connected types of the battery are lead-acid batteries (PbAc), vanadium redox batteries (VRB), lithium-ion batteries (LIB), and sodium-sulfur batteries (NaS). However, one of the main issues being tackled is degradation of the battery efficiency. There are several factors causing degradation of the battery such as battery age, current, discharge/charge voltage, temperature, and the level of discharging/charging [34,35]. Additionally, the factors effecting the life of the battery can be broadly categorized as battery storage period, i.e., environmental factors, and during usage, i.e., cycling conditions. In this paper the battery energy storage system has been considered and it plays a very important role in achieving power sharing during islanded mode of operations.

As shown in Figure 4. The Battery energy storage system is connected with the solar PV system through a bidirectional converter (DC to DC converter), the bidirectional DC to DC converter is further connected to the DC-link and the battery equivalent circuit is shown in Figure 5. Equations relating to the characteristics of the battery are defined in this section. Additionally, the parameters of the battery are given in Table 5.

Table 5. Parameters of BESS.

Parameters	Values	Parameters	Values
C_{b1}	49,000 F	R_{b3}	0.0019 Ω
C_{b2}	1.5 F	R_{b4}	0.045 Ω
R_{b1}	0.045 Ω	V_b	46V
R_{b2}	0.001 Ω		

Where V_b and V_{bt} represents the terminal Voltage and the internal source voltage (V), R_{b1} represents the internal source resistance (Ω) and C_{b1} represents internal capacitance (F), V_{cb1} represents the Voltage (V) across C_{b1} . Where I_{b1} represents internal battery current (A), R_{b2} represents poarization resistance (Ω) and R_{b3} represents ohmic resistance (Ω), which are connected to the charging and discharging properties of the battery, i.e., transient dynamics

respectively. C_{b2} represents the polarization capacitance (F) and V_{cb2} represents Voltage (V) across C_{b2} . Additionally, I_b represents the battery output Current (I). Equations related to the dynamic model of the battery can be expressed in the following equations [36,37].

$$\left. \begin{aligned} R_{b1}I_{b1} - V_{b1} - V_{cb1} &= 0 \\ R_{b2}I_{b2} - V_{cb2} &= 0 \\ V_{cb1} + V_{cb2} + (R_{b3} + R_{b4})I_b + V_b &= 0 \\ I_{b1} &= I_b - C_{b1}pV_{cb1} \\ I_{b2} &= I_b - C_{b2}pV_{cb2} \end{aligned} \right\} \quad (9)$$

$$\left. \begin{aligned} R_{b1}(I_b - C_{b1}pV_{cb1}) - V_{b1} + V_{cb1} &= 0 \\ R_{b2}(I_b - C_{b2}pV_{cb2}) - V_{cb2} &= 0 \\ V_b = -V_{cb1} - V_{cb2} - (R_{b3} + R_{b4})I_b & \end{aligned} \right\} \quad (10)$$

$$\left. \begin{aligned} R_{b1}C_{b1}pV_{cb1} = R_{b1}I_b - V_{b1} - V_{cb1} &= 0 \\ R_{b2}C_{b2}pV_{cb2} = R_{b2}I_b - V_{cb2} & \\ V_b = -V_{cb1} - V_{cb2} - (R_{b3} + R_{b4})I_b & \end{aligned} \right\} \quad (11)$$

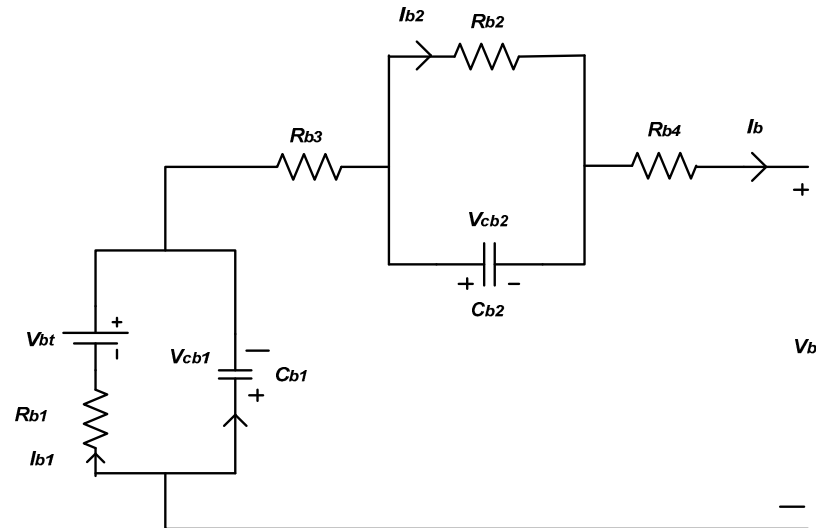


Figure 5. Battery equivalent circuit [37].

The bidirectional boost converter for the battery is given by
 When S_2 is on ($S_2 = 1, S_3 = 0$)

$$C_b pV_b = I_b - I_2 \quad (12)$$

$$V_b - V_{dc} = L_2 pI_2 + R_2 I_2 \quad (13)$$

When S_2 is off ($S_2 = 0, S_3 = 1$)

$$C_b pV_b = I_b - I_2 \quad (14)$$

$$V_b = L_2 pI_2 + R_2 I_2 \quad (15)$$

After combination of the two modes of operation ($S_3 = 1 - S_2$)

$$C_b pV_b = I_b - I_2 \quad (16)$$

$$V_b - S_2 V_{dc} = L_2 pI_2 + R_2 I_2 \quad (17)$$

From the above the DC link voltage equation can be given as

$$C_{dc}pV_{dc} = (1 - S_1)I_1 + S_2I_2 - I_{in} = (1 - S_1)I_1 + S_2I_2 - \frac{3}{4}(M_{q1}I_{s1q} + M_{d1}I_{s1d}) \quad (18)$$

2.2. Modelling and Control of WIND Turbine Generator

Nowadays, the use and development of renewable energy sources such as geothermal, Solar and wind has become very popular and has been introduced worldwide. Like other sources, energy generation from the wind has been remarkably popularized and have been improved and developed since the last decade. Mostly wind turbines are either synchronous generator based or doubly fed induction generator (variable speed) type. Additionally, Permanent magnet (PM) based wind turbine generators are commonly used in wind turbine applications due to the nature of excitation free operations; Also, it offers high efficiency and reliability compared to the other generators [38–40]. Permanent magnet synchronous machines are divided into two; one, permanent magnet (surface mounted) machines (SPM) and two, interior (or buried) permanent magnet machines (IPM). In SPM, the magnets are properly installed on the rotor surface. Thus, the saliency effect becomes negligible. However, in the IPM, saliency effect occurs due to non-uniform equivalent air gap. Therefore, in comparison, the IPM machine has advantages such as solid and robust structure, physically protected and contained magnets. Additionally, the generated magnetic torque and generated reluctance produces higher efficiency and allows the machine to operate in a wider range of speed. Due to this, the IPM model is considered in this paper and the AC-DC-AC converter is used between the main grid and the wind turbine [41,42].

The basic diagram of the IPM wind turbine system is shown in Figure 6. The wind turbine basically consists of blades, generator and converters. For design purpose a three-blade horizontally mount wind turbine is considered. Similar to the other wind turbine system, an IPM utilizes the mechanical energy of the gear system which is converted from the shaft of the turbine blades, the wind turbine converts further the mechanical energy into electrical energy, which is connected further to the electrical system through machine side converter (MSC, i.e., AC to DC converter) and Grid side converter (GSC, i.e., DC to AC converter). As shown in the figure, the GSC and the MSC are connected with the IPM. The MSC controls the speed of the wind turbine rotor and tracks maximum power point of the available power and minimizes the power losses. On the other hand, the grid side converter (GSC) maintains the DC link voltage and controls the flow of the reactive power to the grid as per system requirement [43,44].

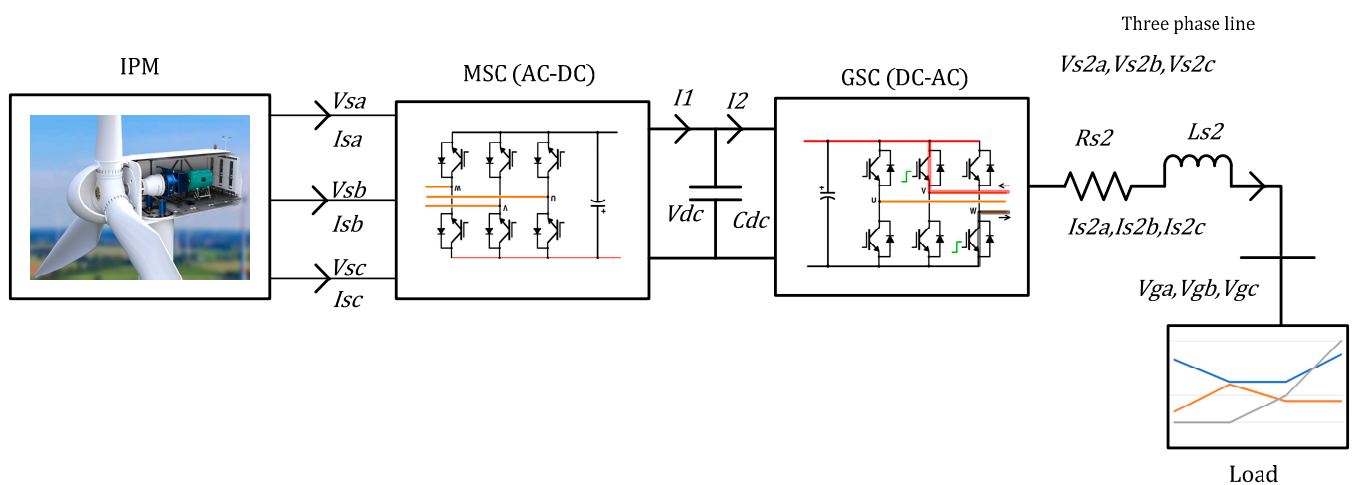


Figure 6. The basic diagram of the IPM wind turbine system.

The main focus relating to control of the wind turbine is to attain maximum available power from the wind while maintaining constant voltage at the DC link, one of the

other important factors is assurance of unity power factor. The power and torque can be calculated as follows

$$P_T = \frac{1}{2} \rho A C_P(\lambda, \beta) V_w^3 \quad (19)$$

$$T_T = \frac{1}{2 \omega_T} \rho A C_P(\lambda, \beta) V_w^3 \quad (20)$$

$$\lambda = \frac{R \omega_T}{V_W} \quad (21)$$

$$C_p = 0.5 \left(\lambda - 0.022 \beta^2 - 5.6 \right) e^{(-0.17 \lambda)} \quad (22)$$

where ρ is the air density, V_W is the wind speed, $A (= \pi R^2)$ is area swept by the rotor, R is the turbine rotor radius, λ is tip speed ratio, ω_T is the angular speed of the wind turbine shaft, β is the rotor blade pitch angle, and C_P is the power coefficient [45,46]. The parameters of the wind turbine are shown in Table 6.

Table 6. Parameters of the wind turbine.

Parameters	Values	Parameters	Values
$V_{w-rated}$	8.5 m/s	β	0 deg
P	1.204 kg/m ³	n_{gear}	5.8
R	4.6	$P_{T-rated}$	22.9 kW

3. Control Unit Diagram

The generalized droop control (GDC) unit diagram for the microgrid system is shown in Figure 7, the output DC voltage from the RES is converted to AC voltage through GDC, the voltage magnitude and frequency of each DG units are in line with the characteristics of the total load. The converter is fed by an important feedback loop, the feedback loop consists of four major important parts, such as droop controller, mainly to ascertain total power balance between generation and load. The droop control controls the voltage and frequency of the corresponding output reactive and active power of the converter. The voltage control and the current control maintains the control voltage and current up to the limit and finally a phase lock loop (PLL) measures the local frequency while aligning the load voltage in reference frame of the q-axis [47,48].

3.1. Generalized Droop Control (GDC)

The droop control is commonly used in many power generating plants, by drooping the frequency, the total active power of the load is distributed on various generations generally related to the frequency and considered as converter output active power function. Similarly, the magnitude of voltage output of the converter is considered as a function of the output reactive power, this can also be drooped as per requirement so as that the total reactive power of the load is distributed among the DGs. This method provides sharing of total load as well as control the required operational range of voltage and frequency in the system. Generally, the cut of frequency is considered to be around 10% of the nominal frequency, this is assumed to be reliable for producing the average output power value and eliminating fluctuations [49,50].

Let us consider a simple structure of a single DG system as shown in Figure 8. The circuit shows that a DG unit, i.e., DG1 is applied to the load, and V_2 is considered the voltage at PCC located on the load side; the voltage source converter (VSC) transforms the DC voltage into AC, as per the system requirement, and the output voltage V_1 is considered at point A; the line impedance Z_L , the reactive power Q_A , and real power P_A at point A can be given by.

$$P_A = \frac{V_1}{R_L^2 + X_L^2} [R_L (V_1 - V_2 \cos \delta) + X_L V_2 \sin \delta] \quad (23)$$

$$Q_A = \frac{V_1}{R_L^2 + X_L^2} [-R_L V_2 \sin \delta + X_L (V_1 - V_2 \cos \delta)] \quad (24)$$

where P_A represents real power, and Q_A is the reactive power, V_1 represents inverter output voltage at point A, V_2 is the voltage at PCC and δ represents power angle and θ represents the phase angle of the line impedance Z_L , also, X_L and R_L represents the line reactance as well as inductance of the line. In general, either X_L or R_L is ignored in Equations (23) and (24), by neglecting reactance and inductance of the line the P-V/Q-f or P-f/Q-V relation of the droop characteristics are developed. Additionally, the virtual reactive power Q_{vir} as well as the real power P_{vir} can be derived as,

$$P_{vir} = \frac{X_L}{Z_L} P_A - \frac{R_L}{Z_L} Q_A \quad (25)$$

$$Q_{vir} = \frac{R_L}{Z_L} P_A - \frac{X_L}{Z_L} Q_A \quad (26)$$

From above, Equations (23) and (24) becomes

$$\delta = \frac{Z_L P_{vir}}{V_1 V_2} \quad (27)$$

$$V_1 - V_2 = \frac{Z_L Q_{vir}}{V_1} \quad (28)$$

From the above equation, the P_{vir} and Q_{vir} can be used to regulate the frequency and voltage of the microgrid system. Therefore, the generalized droop relation becomes

$$f = f^* - k_{pf}(P_{vir} - P^*) \quad (29)$$

$$V = V^* - k_{qv}(Q_{vir} - Q^*) \quad (30)$$

Also, from the above equations, we have droop control relations

$$\Delta f = \frac{1}{K_f} \left(\frac{Z}{X} P' - P_0 \right) + K_R K_V \Delta V_s + K_R Q_0 \quad (31)$$

$$\Delta V_s = \frac{1}{K_v} \left(\frac{Z}{X} Q' - Q_0 \right) - K_R K_f \Delta f + K_R P_0 \quad (32)$$

3.2. Simulation of the GDC System

After careful implementation of the intake microgrid system, simulation has been done and the following figure shows the simulation result of the GDC Intake microgrid system during grid connected mode and islanded mode of operations, Figure 9 shows the Load power vs. source power graph, where battery power compensates the power flow as per requirements. Figure 10 shows the V&I vs. Time at the point of common coupling, where sudden change in current is seen at 0.5 s. Figure 11 shows the modulation index waveform of the inverter side control schemes. Additionally, Figure 12 shows the DC link voltage with at different switching time, i.e., grid connected mode and islanded mode. Figure 13 shows the frequency response of the microgrid system under switching conditions. Figure 14 represents the reactive power as well as the active power response of the microgrid system.

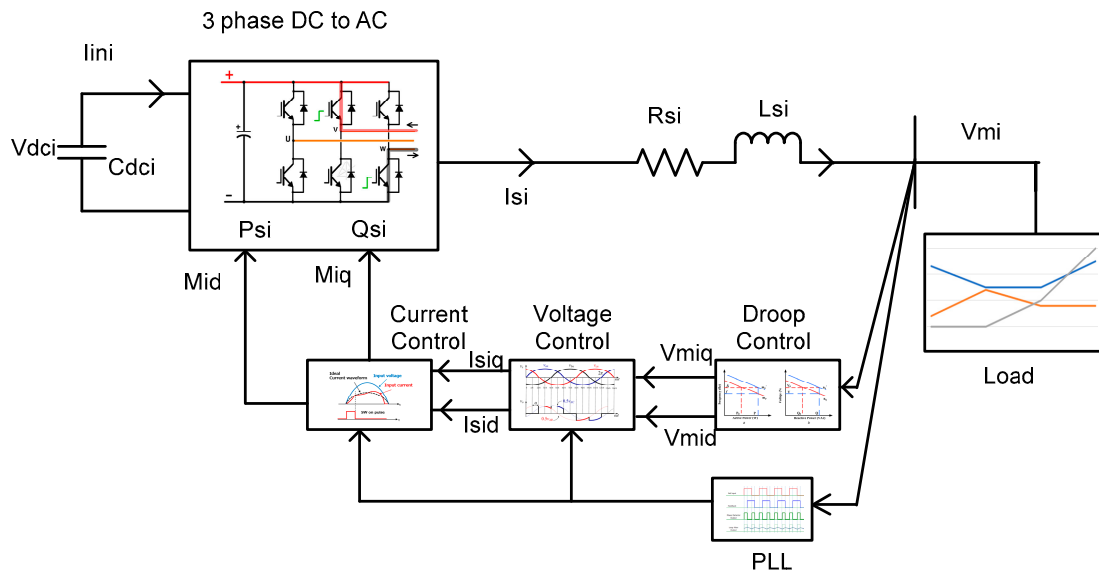


Figure 7. GDC unit diagram.

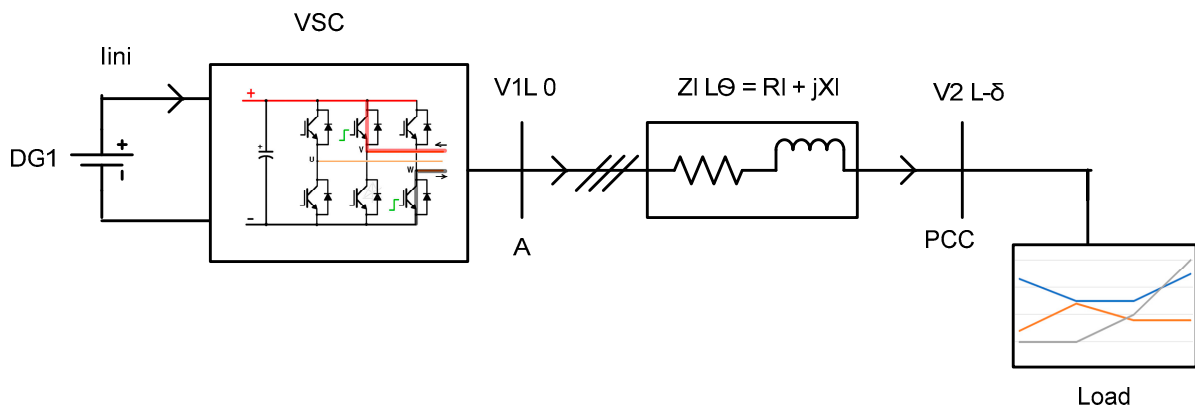


Figure 8. Structure of a single DG system.

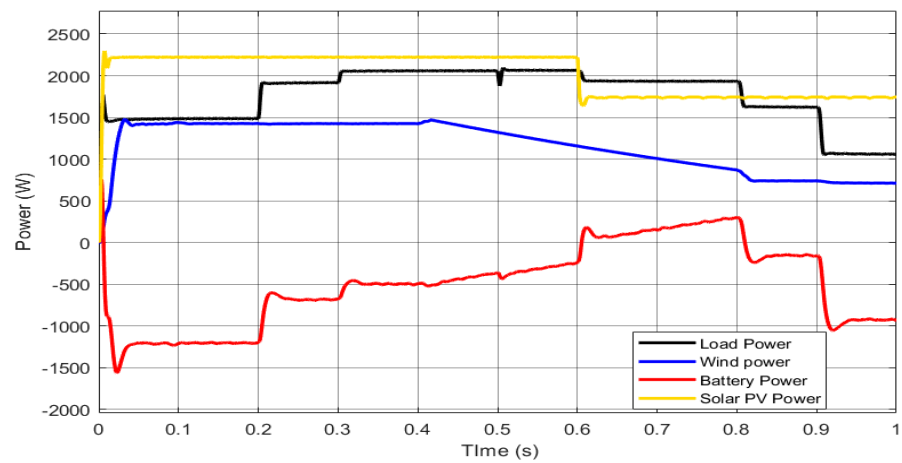


Figure 9. Load vs. Source power.

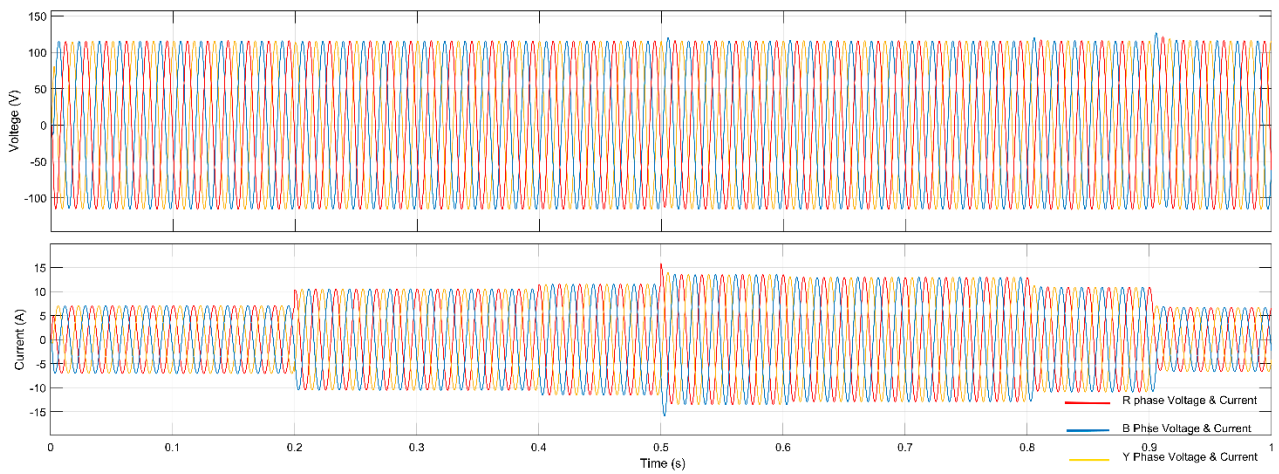


Figure 10. V&I at point of common coupling (PCC).

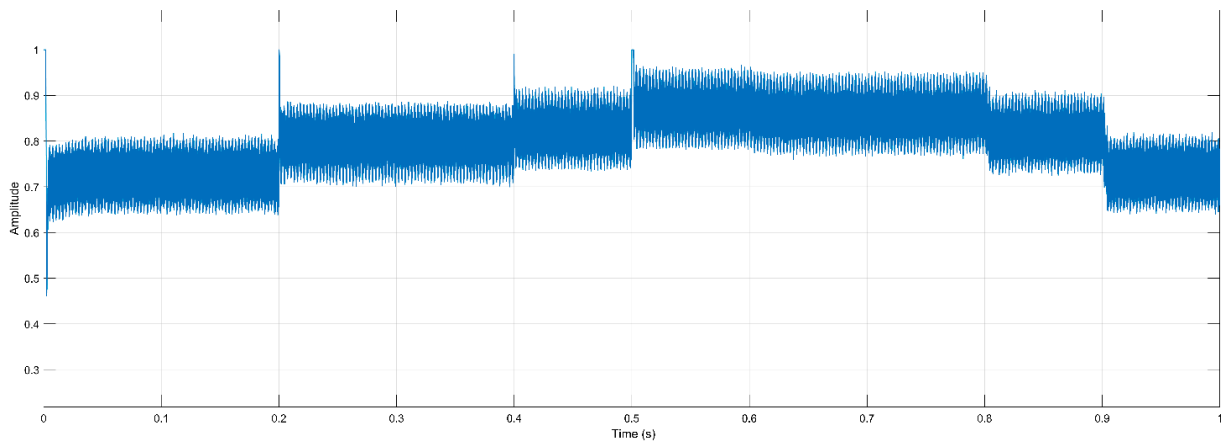


Figure 11. Modulation index waveform.

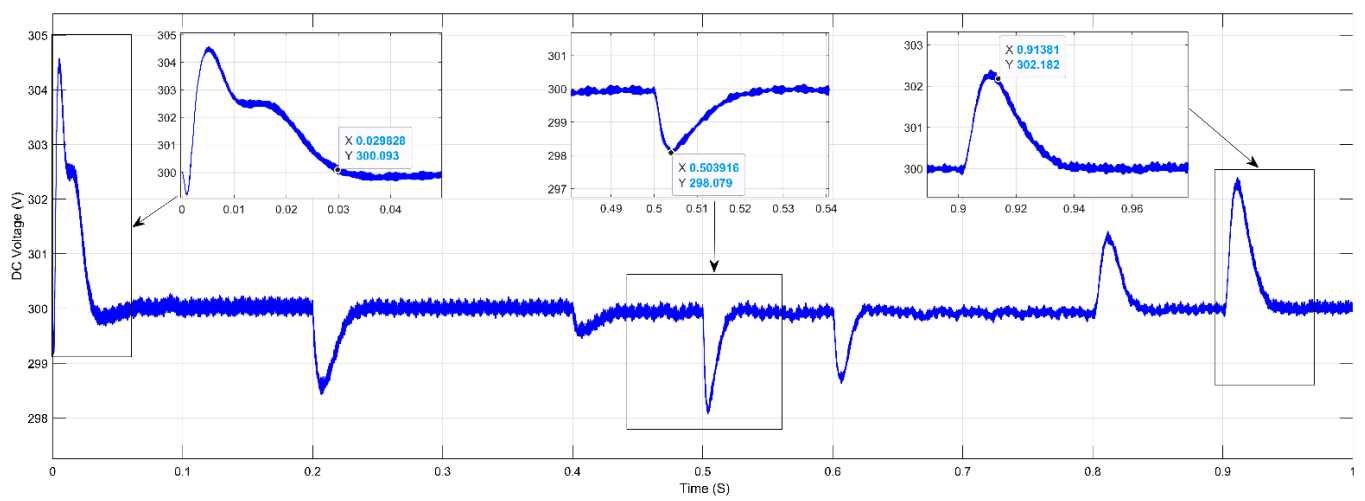


Figure 12. DC link voltage.

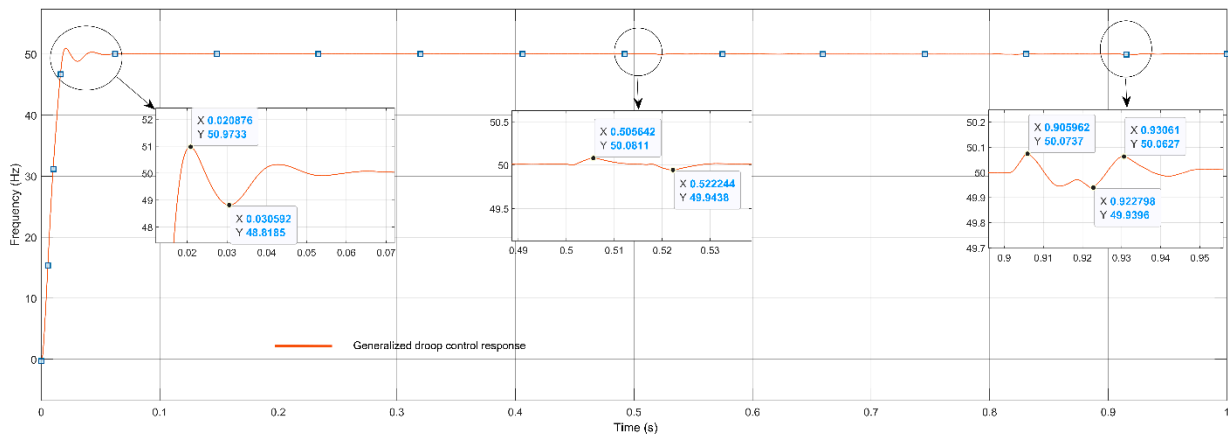


Figure 13. GDC Frequency.

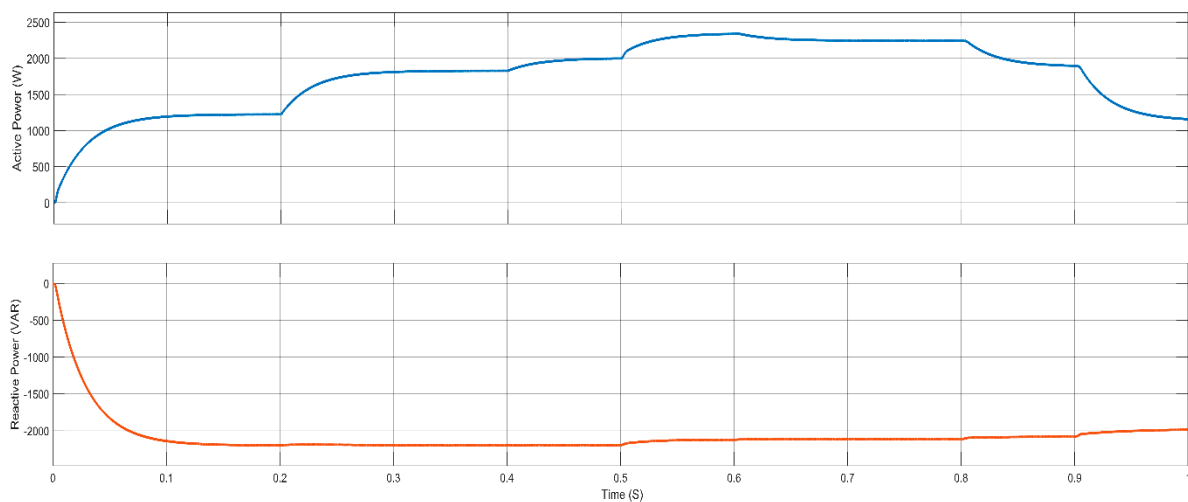


Figure 14. Active and Reactive Power.

From the figure we can observed the corresponding change in solar power, wind power and battery power under switching of various load demand. It can be seen that during off peak conditions, the battery continuously charges to balance the power flow while maintaining the frequency. Further, after a near nominal frequency is attained the battery begin to charge. From the general power flow graph, it can be seen that the generalized droop control scheme shows good results in grid-connected mode of operation. However, when the microgrid is switched to islanded mode, severe fluctuation may happen if the line parameters are not properly set. Additionally, some study shows that sharing of actual real and reactive power may become an issue due to high reliability on the output impedance and line impedance between DG units and load [51,52]. Therefore, in order to resolve this issue, a new intelligent approach by adopting ANFIS-based microgrid system is proposed and explained in the below section.

4. ANFIS-Based Droop Control Approach

ANFIS Architecture and Controller

ANFIS falls under the category of an Artificial Intelligence (AI) system and it is a hybrid combination of Neural Networks (NN) and Fuzzy Logic (FL) technique. It is generally used in various fields for solving complex and nonlinear systems. The ANFIS provides an adaptive modelling method for learning information from the set of input data. The membership functions (MFs) and Fuzzy rules are obtained by training the system using selected data sets, during the training process the parameters of the MFs can be adjusted

accordingly. Additionally, hybrid or back propagation learning methods are used so as to determine the parameters of the adaptive system.

In this paper, the trained ANFIS has two input data, i.e., active power (P) and reactive power (Q) where the corresponding output are frequency (f) and Voltage (V). different learning algorithm, i.e., hybrid algorithm for each input is used in order to determine the parameters, one of the advantages of using ANFIS is non requirement of previously obtained information about the MFs rules if the ANN are properly tuned. Additionally, the ANFIS can selects the MFs parameters automatically based on requirement. The parameters of the MFs are set and determined by using Product of two sigmoidal membership function (psigmf) and the Triangular membership function (trimf) method.

The typical ANFIS structure shown in Figure 15 has Multi Input Single Output (MISO) structure and the structure contains five layers, where P and Q are the two active and reactive power inputs. Additionally, A1 and A2 represents the membership functions of input P, whereas B1 and B2 represents the membership functions of input Q. The First layer represents the membership function of each individual inputs. Additionally, AND operation is performed in the second layer for both the MFs of input one and input two, the corresponding rules for the input could be formed as follows; [53,54].

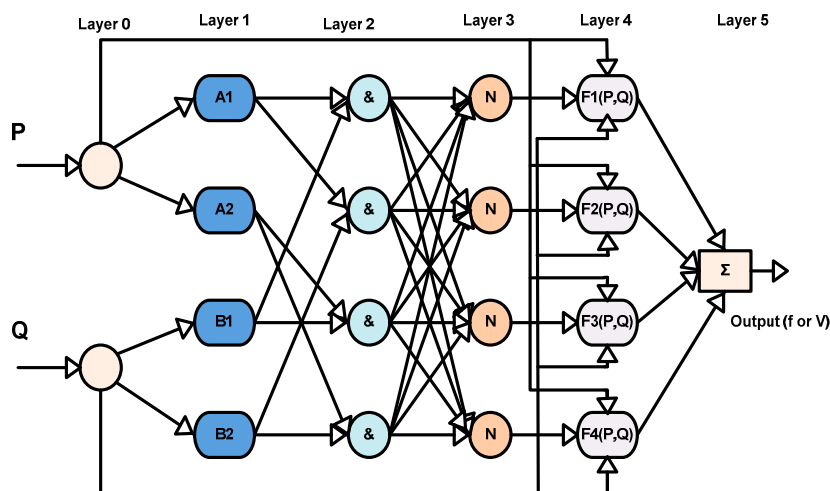


Figure 15. ANFIS typical structure.

- Rule no 1: If P is A₁ and Q is B₁, then $f_1 = p_1P + q_1Q + r_1$,
- Rule no 2: If P is A₂ and Q is B₂, then $f_2 = p_2P + q_2Q + r_2$.

From the above rules, p_1, q_1, r_1 and p_2, q_2, r_2 represents the parameters of each of the output functions. Each node of these output is referred as firing strength of a rule. The corresponding layers of the ANFIS are explained in the followings

Layer 1: Every node in the first layer represents a square node containing a node functions, the fuzzy sets are obtained by applying the input variables, which are in proportional to the input variables. Each node representing as an I in the layers have a function representing the membership value of each input, the corresponding node output are described as follows

$$\left. \begin{aligned} O_{1,i} &= \mu_{A_i}(P); i = 1, 2 \\ O_{1,i} &= \mu_{B_{i-2}}(Q); i = 3, 4 \end{aligned} \right\} \tag{33}$$

where Q and P represents the input of node i, B_i (or A_i) represents the linguistic label (could be small, large, etc.). Additionally, it can be stated that O_{1,i} is the MF of A_i. and it specifies the degree to which it satisfies the quantifier A_i. Normally, μ_{A_i} is selected in a bell-shaped

form containing a limit set of 1 as maximum and 0 as minimum correspondingly, $\mu A_i(P)$ can be given as follows [55,56]

$$\mu A_i(P) = \frac{1}{1 + \left(\frac{P-c_i}{\alpha_i}\right)^{2\beta}} \quad (34)$$

where α_i, β_i, c_i are known as the premise parameters and are called parameter set, as the values of these parameters change, they exhibit several forms of membership functions on A_i or linguistic label.

Layer 2: Every node in the second layer is a multiplication of the output of first layer and sends the product out. It can be represented as,

$$Q_{2,i} = W_i = \mu A_i(P) \times \mu B_i(Q); i = 1,2 \quad (35)$$

Each node output represents the firing strength of a rule, i.e., W_i . The signals from the incoming are i th line with the precursor (if) of the rule.

Layer 3: In the third layer, every node represents a circle node written as N . the activity of each and every rule is considered. The number of fuzzy rules and the number of layers is equal. This layer output is considered as a regularized form of the previous layer. The i th node computes the ratio of the i th rule's firing strength against all rule's firing strengths, as shown below [57].

$$O_{3,i} = \bar{w}_i \frac{w_i}{\sum_j w_j} \quad (36)$$

Layer 4: In fourth layer, the products are the fractional output values, i.e., from layer 0 and layer 3, the output node i are Takagi-Sugeno type represented as follows

$$O_{4,i} = \bar{w}_i f_i = \bar{w}_i (p_i P + q_i Q + r_i) \quad (37)$$

Whereas, \bar{w}_i is the output of the fourth layer, p_i, q_i, r_i are the parameter set, denoted as consequent parameters

Layer 5: The final ANFIS output is obtained in the fifth layer. The output is nothing but the summation of the incoming signals from the layer four as shown below.

$$O_5 = \sum_i \bar{w}_i f_i \quad (38)$$

The fifth layer is nothing but the defuzzification layer, this fifth layer computes the result of the previous layers and the ANFIS output, the node function contains almost no constraints except piecewise differentiability in an adaptive network. Additionally, the one constraint in the adaptive network configuration is that it should be a feedforward type. Due to these constraints, applications are instantaneous and vast in many areas. Implementation of ANFIS and Validation

In order to implement the ANFIS-based controller, the generalized droop control structure, shown in the Figure 7 can be remodelled by ANFIS as shown in Figure 16. Therefore, after ensuring the validity of the model, the proposed ANFIS-based controller could be used for droop control as shown in the figure.

After implementation of the ANFIS-based droop control model, the input and output data set are used for training the ANFIS, the droop control unit consists two input data, i.e., active and reactive power and two output data, i.e., frequency and voltage amplitude, separately. In order to smoothly carry out the operations, two ANFIS blocks are individually applied for controlling the voltage and frequency outputs. Additionally, ANFIS operates on multi-input-single-output (MISO) signals only. The input and output data set are generated and stored in the system, and the corresponding ANFIS models are generated and trained. After continuous training of the ANFIS, the error tolerance values are evaluated and minimal training RMSE result shows that ANFIS has been trained successfully. Therefore, after successful training, the conventional controllers are now been replaced with the trained

ANFIS controllers, the active and reactive loads are then changed by switching various loads and the system output frequency and voltage are compared to the conventional droop results. ANFIS training data for the frequency control as well as voltage control are shown in the Tables 7 and 8 below.

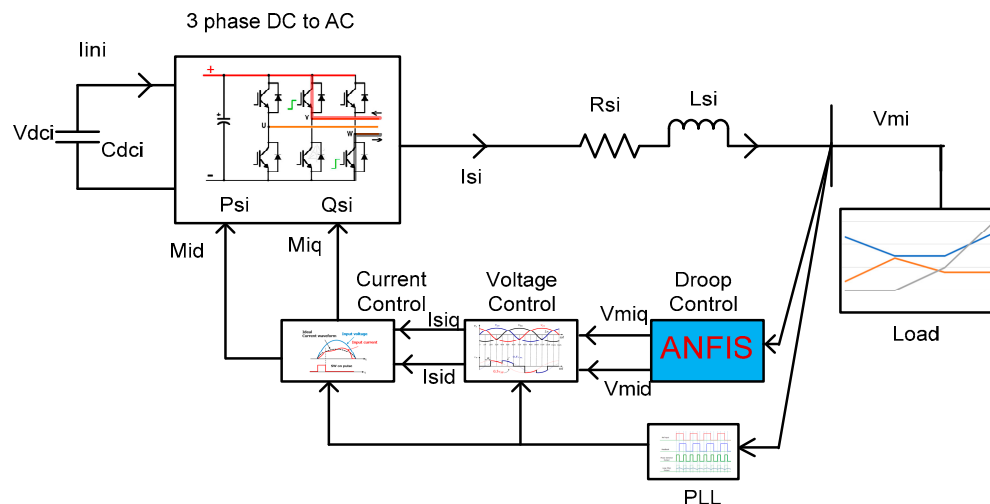


Figure 16. ANFIS droop control model.

Table 7. ANFIS train data: for frequency control.

Sl. No.	Details	Data	Details	Data
1	Input Numbers of MFs	63	Error tolerance	0
2	Input MFs type	Product of two sigmoidal membership function (psigmf)	Epochs	200
3	Output MFs type	Constant	Optimization method	Hybrid

Table 8. ANFIS train data: for Voltage control.

Sl. No.	Details	Data	Details	Data
1	Input Numbers of MFs	63	Error tolerance	0
2	Input MFs type	Triangular membership function (trimf)	Epochs	200
3	Output MFs type	Linear	Optimization method	Hybrid

Here, the Membership Functions data for frequency and Voltage are carefully chosen, such as input number of Membership Functions (MFs), Input MFs type are carefully chosen and compared with other combination options such as Triangular membership function (trimf), trapezoidal membership function (trapmf), Generalized bell-shaped membership function (gbellmf), Gaussian membership function (gaussmf), Gaussian combination membership function (gauss2mf), pi-shaped membership function (pimf), difference between two sigmoidal membership function (dsigmf). Selection of MFs plays a very important in

choosing the optimal sets of output, each MFs type offers different results as per training procedures. After completion of training different combination of data sets. The ANFIS info such as Number of nodes, Number of linear parameters, Number of nonlinear parameters, Total number of parameters, Number of training data pairs, Number of checking data pairs, and Number of fuzzy rules are compared to see the optimal results and most important of all the lowest Minimal training RMSE is chosen as it shows best results where the selection of zero error tolerance is chosen in training the data sets. After finalization of the required data the optimal ANFIS train data for Frequency and Voltage are selected as shown in the below table. Similarly, the corresponding output P-f and Q-V sets of trained data are shown in Table 9 below.

Table 9. ANFIS structure train data of Q-V and P-F.

Sl. No.	Parameters	P-f ANFIS Data	Q-V ANFIS Data
1	Number of nodes	59	43
2	Number of linear parameters	54	36
3	Number of nonlinear parameters	36	21
4	Total number of parameters	90	57
5	Number of training data pairs	500172	500,172
6	Number of fuzzy rules	18	12
7	Number of checking data pairs	0	0
8	Minimal training RMSE	0.002753	0.001753

5. Results and Discussion

In order to understand the characteristics and efficiency of the proposed ANFIS system, the controller output of the droop controller, i.e., P&Q are trained with ANFIS function, after several attempts and successful training, the corresponding controllers are set and tuned in the Simulink model and simulations were performed in MATLAB Simulink environment under different loading conditions (i.e., varying load demand). During this simulation period, the microgrid system operates in grid connected mode for 0–0.5 s and 0.5–1 s in islanded mode of operation. The results are compared with GDC results which are shown in the previous sections and the corresponding DC link voltage, frequency response, active and reactive power are shown in Figures 17–19.

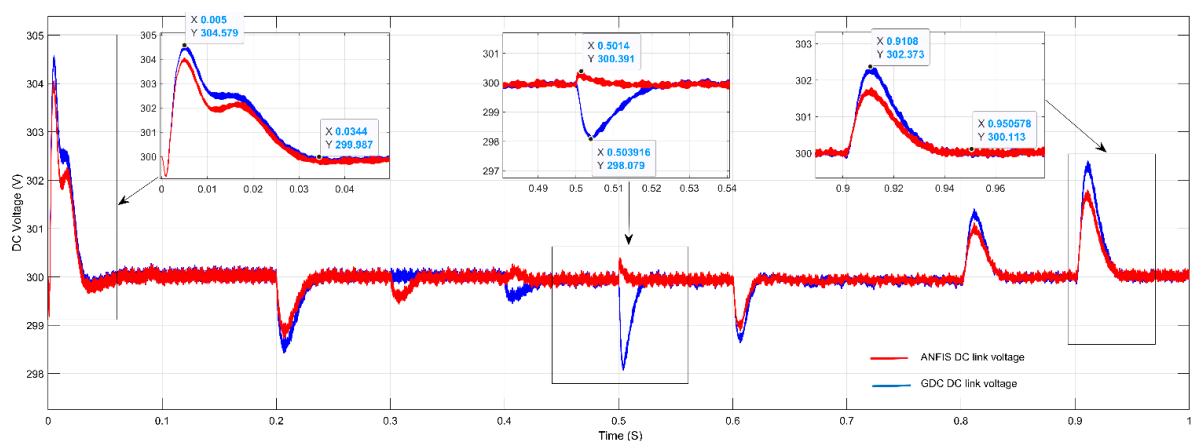


Figure 17. Comparison of DC link voltage.

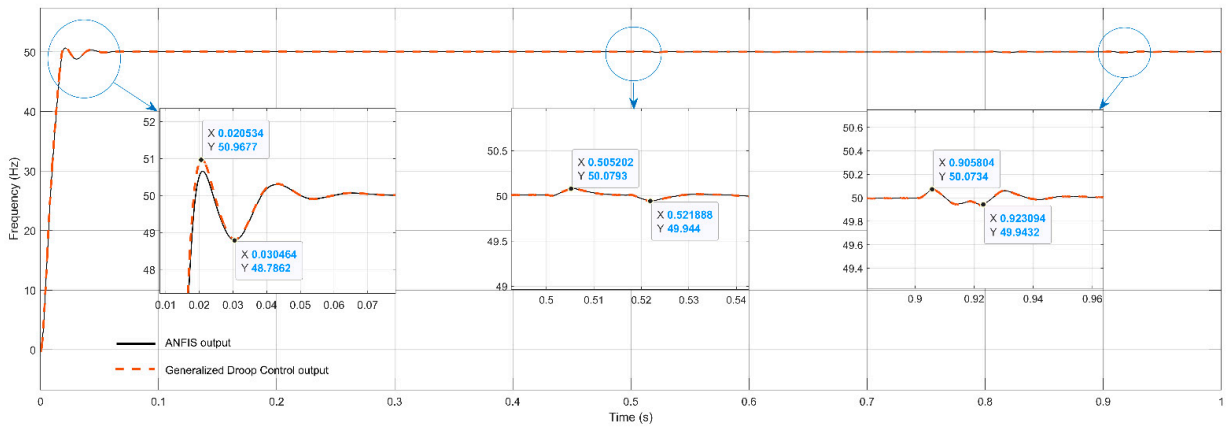


Figure 18. Comparison of Frequency GDC vs. ANFIS.

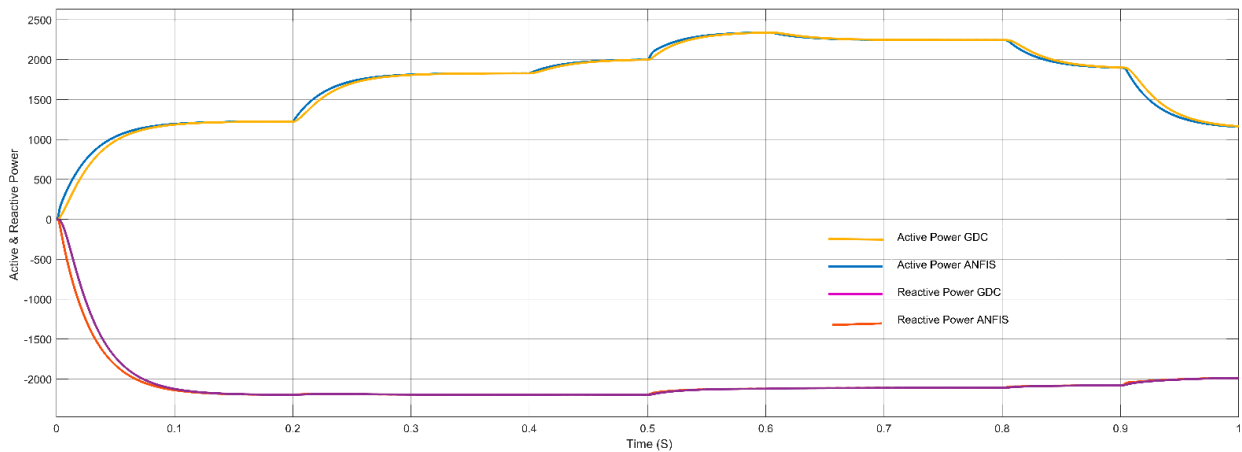


Figure 19. Comparison of Active and Reactive power vs. Time.

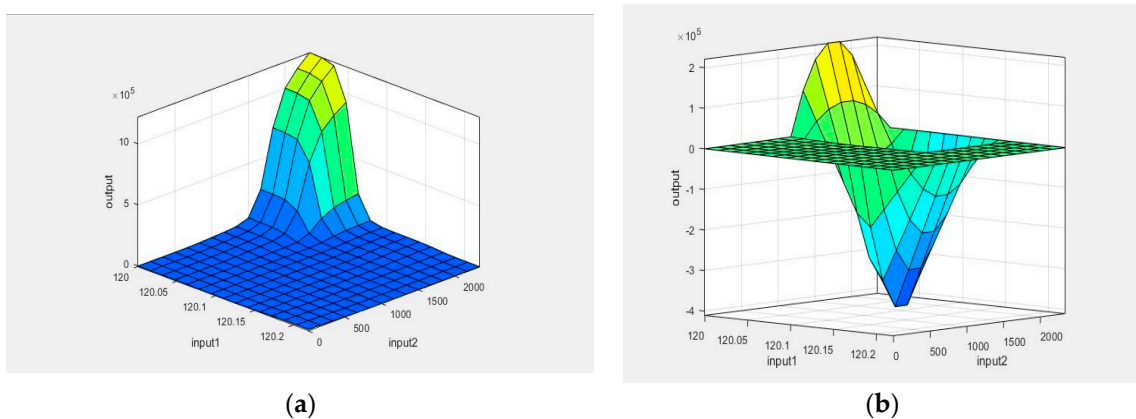


Figure 20. Surface plot. (a) P-F ANFIS; (b) Q-V ANFIS.

The comparison results of DC link voltage shown in Figure 20 represents that ANFIS improves the output DC link voltage by reducing the transient during switching operations under grid connected and islanded mode of operations. Similarly, Figure 21 shows improvement in frequency by reducing the frequency deviations during different switching conditions. Additionally, Figure 22 indicates improvement in active power (P) and reactive power (Q) under ANFIS method. Apart from the above, various system responses under ANFIS droop technique have been studied, and the system shows better and reliable results compared to GDC considering different switching timeframes.

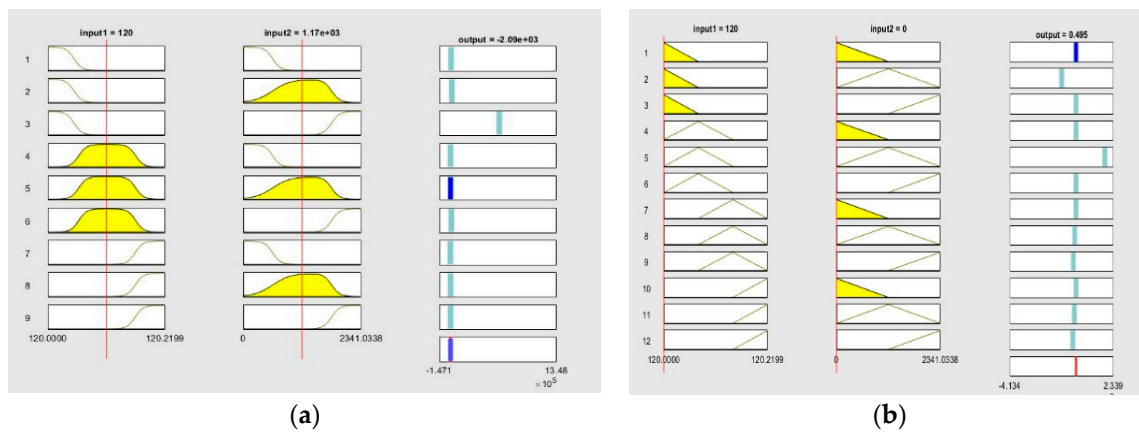


Figure 21. Fuzzy rules. (a) P-F ANFIS; (b) Q-V ANFIS.

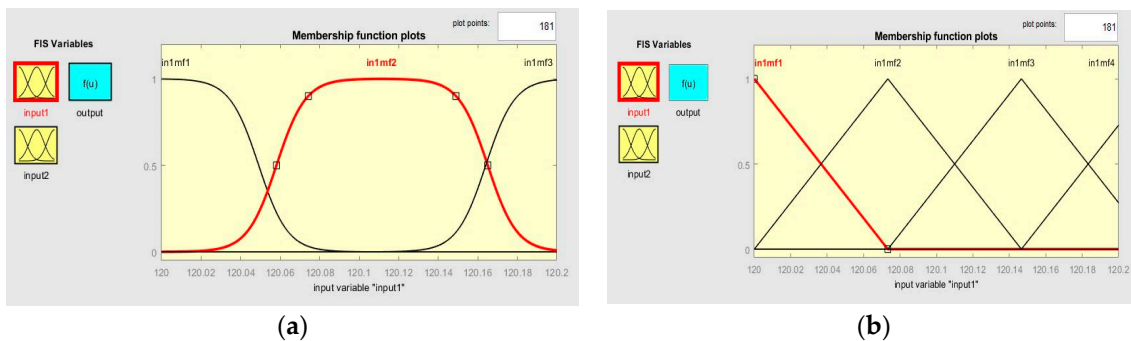


Figure 22. Membership function plot. (a) P-F ANFIS; (b) Q-V ANFIS.

6. Conclusions

In this paper ANFIS-based Droop control technique considering intake microgrid system was analyzed under different loading conditions, which is considered analogous to different loadings of intake system. Similarly, in order to compare and analyze the results, the conventional droop control technique using generalized droop control (GDC) technique has also been considered. Simulation results were shown for different loading conditions. ANFIS has been successfully trained for considering both the cases of P-f and Q-V droop separately. Moreover, the controller block for both the P-f and Q-V droop are replaced with trained ANFIS controllers, and simulations were drawn for different loading conditions. GDC seems to show acceptable results under grid connected and islanded mode of operations, the corresponding graphs such as load vs. source power, V&I at PCC, Modulation index, DC link voltage, frequency, and active and reactive power were observed, and the system seems to show good results; however, transient behavior during switching may disturb the system and may even cause unwanted issues. In grid-connected mode, power sharing of active and reactive powers between source and load plays a very important role, whereas, in islanded mode, control of the system frequency and voltage becomes the main challenge and ANFIS-based droop control technique was considered for solving this issue. As the intake contains both the HT load and LT loads, only the LT side of the load has been considered in the simulation. The designed system operates in grid connected mode for 0.5 s and islanded mode for 1 s. As various load changes the battery system compensates the overall power sharing between source and load. The trained ANFIS data such as surface plot, fuzzy rules, membership function plot and RMSE value of both the P-f and Q-V droop shows successful training of the ANFIS and the corresponding application was made by replacing both the controller units of P-f and Q-V.

Considering the stability of the proposed microgrid system, frequency plays a very important role in analysis of the system performance. In fact, in the droop control technique, the frequency of the system is highly depending on the active power balance between load

and source. In the proposed intake microgrid system, batteries play a very important role, and it injects and absorbs the real power during frequency imbalance. Additionally, the system voltage is highly depending on the reactive power balance between the source and load. The proposed ANFIS-based droop controller seems to show good results in regulating the frequency, as well as voltage of an intake microgrid system. The reliability has been tested by comparing the performance of the GDC, and it has been tested in different loading conditions. The comparison of the simulation results shows satisfactory performance of the ANFIS system.

As far as the consideration of water treatment plant-based intake microgrid is concerned, the same concept could be useful for solving various issues being faced in various water treatment plants, such as huge operational costs, power-related issues, frequent maintenance, etc. By adapting the same technique, ANFIS-based droop control could also be used in several treatment plants similar to waste water treatment such as sewage treatment, etc.

Author Contributions: Conceptualization, S.D.; Data curation, N.S.; Formal analysis, C.R. and A.K.; Funding acquisition, A.K.; Methodology, T.S.U.; Project administration, T.S.U.; Supervision, T.S.U. All authors have read and agreed to the published version of the manuscript.

Funding: This research received no external funding.

Conflicts of Interest: The authors declare no conflict of interest.

References

1. Yoldas, Y.; Goren, S.; Onen, A.; Ustun, T.S. Dynamic rolling horizon control approach for a university campus. *Energy Rep.* **2022**, *8*, 1154–1162. [[CrossRef](#)]
2. Latif, A.; Hussain, S.S.; Das, D.C.; Ustun, T.S. Optimum Synthesis of a BOA Optimized Novel Dual-Stage $PI - (1 + ID)$ Controller for Frequency Response of a Microgrid. *Energies* **2020**, *13*, 3446. [[CrossRef](#)]
3. Guerrero, J.M.; Vasquez, J.C.; Matas, J.; de Vicuña, L.G.; Castilla, M. Hierarchical control of droop-controlled AC and DC microgrids—A general approach toward standardization. *IEEE Trans. Ind. Electron.* **2011**, *58*, 158–172. [[CrossRef](#)]
4. Majumder, R.; Ghosh, A.; Ledwich, G.; Zare, F. Power Management and Power Flow Control with Back-to-Back Converters in a Utility Connected Microgrid. *IEEE Trans. Power Syst.* **2010**, *25*, 821–834. [[CrossRef](#)]
5. Hu, J.F.; Zhu, J.G.; Platt, G. A droop control strategy of parallel-inverter-based microgrid. In Proceedings of the 2011 International Conference on Applied Superconductivity and Electromagnetic Devices, Sydney, Australia, 14–16 December 2011; pp. 188–191.
6. Zhong, Q.C. Robust Droop Controller for Accurate Proportional Load Sharing Among Inverters Operated in Parallel. *IEEE Trans. Ind. Electron.* **2013**, *4*, 1281–1290. [[CrossRef](#)]
7. Ali, A.; Li, W.; Hussain, R.; He, X.; Williams, B.W.; Memon, A.H. Overview of current microgrid policies, incentives and barriers in the European union, united states and china. *Sustainability* **2017**, *9*, 1146. [[CrossRef](#)]
8. Vigneysh, T.; Kumarappan, N.; Arulraj, R. Operation and control of wind/fuel cell based hybrid microgrid in grid connected mode. In Proceedings of the International Conference on Automation, Computing, Communication, Control and Compressed Sensing, Kottayam, India, 22–23 March 2013; pp. 754–758.
9. Li, Y.; Li, Y.W. Power Management of Inverter Interfaced Autonomous Microgrid Based on Virtual Frequency-Voltage Frame. *IEEE Trans. Smart Grid* **2011**, *2*, 30–40. [[CrossRef](#)]
10. Vigneysh, T.; Kumarappan, N. Autonomous operation and control of photovoltaic/solid oxide fuel cell/battery energy storage based microgrid using fuzzy logic controller. *Int. J. Hydrogen Energy* **2016**, *41*, 1877–1891. [[CrossRef](#)]
11. Hu, J.; Shan, Y.; Yinliang, X.; Guerrero, J.M. A coordinated control of hybrid ac/dc microgrids with PV-wind-battery under variable generation and load conditions. *Int. J. Electr. Power Energy Syst.* **2019**, *104*, 583–592. [[CrossRef](#)]
12. Tah, A.; Das, D. An Enhanced Droop Control Method for Accurate Load Sharing and Voltage Improvement of Isolated and Interconnected DC Microgrids. *IEEE Trans. Sustain. Energy* **2016**, *7*, 1194–1204.
13. Meng, L.; Tang, F.; Savaghebi, M.; Vasquez, J.C.; Guerrero, J.M. Tertiary Control of Voltage Unbalance Compensation for Optimal Power Quality in Islanded Microgrids. *IEEE Trans. Energy Convers.* **2014**, *29*, 802–815. [[CrossRef](#)]
14. Yoon, C.; Bai, H.; Beres, R.N.; Wang, X.; Bak, C.L.; Blaabjerg, F. Harmonic stability assessment for multi-paralleled grid-connected inverters. In Proceedings of the IEEE International Power Electronics and Application Conference and Exposition, Shanghai, China, 5–8 November 2014; pp. 1098–1103.
15. Rosato, A.; Altilio, R.; Araneo, R.; Panella, M. Prediction in photovoltaic power by neural networks. *Energies* **2017**, *10*, 1003. [[CrossRef](#)]
16. de Matos, J.G.; de Silva, F.S.F.; de S Ribeiro, L.A. Power control in ac isolated microgridss with renewable energy sources and energy storage systems. *IEEE Trans. Ind. Electron.* **2015**, *62*, 3490–3498.

17. Olivares, D.E.; Canizares, C.A.; Kazerani, M.; Mehrizi-Saini, A.; Etemadi, A.H.; Iravani, R.; Hajimiragha, A.H.; Gomis-Bellmunt, O.; Saeedifard, M.; Palma-Behnke, R.; et al. Trends in microgrid control. *IEEE Trans. Smart Grid* **2014**, *5*, 1905–1919. [[CrossRef](#)]
18. Igualada, L.; Corchero, C.; Cruz-Zambrano, M.; Heredia, F.J. Optimal energy management for a residential microgrid including a vehicle-to-grid system. *IEEE Trans. Smart Grid* **2014**, *5*, 2163–2172. [[CrossRef](#)]
19. Bevrani, H.; Shokoohi, S. An Intelligent Droop Control for Simultaneous Voltage and Frequency Regulation in Islanded Microgrids. *IEEE Trans. Smart Grid* **2013**, *4*, 1505–1513. [[CrossRef](#)]
20. Kermani, M. Transient voltage and frequency stability of an isolated microgrid based on energy storage systems. In Proceedings of the 2016 IEEE 16th International Conference on Environment and Electrical Engineering (EEEIC), Florence, Italy, 7–10 June 2016; pp. 1–5.
21. Zou, Z.; Buticchi, G.; Liserre, M.; Kettner, A.M.; Paolone, P. Voltage stability analysis using a complete model of grid-connected voltage source converters. In Proceedings of the 2016 IEEE Energy Conversion Congress and Exposition (ECCE), Milwaukee, WI, USA, 18–22 September 2016; pp. 1–8.
22. Lage, G.G.; Fernandes, R.A.S.; da Costa, G.R.M.; Cao, J. Optimal power flows with voltage stability constraint based on voltage stability indices and artificial neural networks. In Proceedings of the IEEE Power Tech, Eindhoven, The Netherlands, 29 June–2 July 2015.
23. Leonori, S.; De Santis, E.; Rizzi, A.; Frattale Mascioli, F.M. Multi objective optimization of a fuzzy logic controller for energy management in microgrids. In Proceedings of the 2016 IEEE Congress on Evolutionary Computation (CEC), Vancouver, BC, Canada, 24–29 July 2016; pp. 319–326.
24. Nguyen, V.G.; Guo, X.; Zhang, C.; Chen, C.; Tran, N.T. The analysis of electric power steering base on fuzzy-PI control. In Proceedings of the 2017 4th International Conference on Systems and Informatics (ICSAI), Hangzhou, China, 11–13 November 2017; Volume 2018, pp. 121–126.
25. Liu, Y.; Han, Y.; Lin, C.; Yang, P.; Wang, C. Design and Implementation of Droop Control Strategy for DC Microgrid Based on Multiple DC/DC Converters. In Proceedings of the 2019 IEEE Innovative Smart Grid Technologies-Asia (ISGT Asia), Chengdu, China, 21–24 May 2019; pp. 3896–3901.
26. Magdefrau, D.; Taufik, T.; Poshtan, M.; Muscarella, M. Analysis and review of DC microgrid implementations. In Proceedings of the 2016 International Seminar on Application for Technology of Information and Communication (ISemantic), Semarang, Indonesia, 5–6 August 2016; pp. 241–246.
27. Ferdous, S.M. *Operation and Control Strategy of Coupled Microgrid Clusters*; Murdoch University: Perth, Australia, 2021.
28. Planas, E.; Andreu, J.; Gárate, J.I.; De Alegria, I.M.; Ibarra, E. AC and DC technology in microgrids: A review. *Renew. Sustain. Energy Rev.* **2015**, *43*, 726–749. [[CrossRef](#)]
29. Ferdous, S.M.; Shafiqullah, G.M.; Shahnia, F.; Elavarasan, R.M.; Subramaniam, U. Dynamic frequency and overload management in autonomous coupled mgs for self-healing and resiliency improvement. *IEEE Access* **2020**, *8*, 116796–116811. [[CrossRef](#)]
30. Molotov, P.; Vaskov, A.; Tyagunov, M. Modeling Processes in Microgrids with Renewable Energy Sources. In Proceedings of the 2018 International Ural Conference on Green Energy (UralCon), Chelyabinsk, Russia, 4–6 October 2018; pp. 203–208.
31. Thao, N.G.M.; Uchida, K. A two-level control strategy with fuzzy logic for large-scale photovoltaic farms to support grid frequency regulation. *Control Eng. Pract.* **2017**, *59*, 77–99. [[CrossRef](#)]
32. Adhikari, S.; Li, F. Coordinated V_f and PQ control of solar photovoltaic generators with MPPT and battery storage in microgrids. *IEEE Trans. Smart Grid* **2014**, *3*, 1270–1281. [[CrossRef](#)]
33. Kumar, P.S.; Chandrasena, R.P.S.; Ramu, V.; Srinivas, G.N.; Babu, K.V.S.M. Energy Management System for Small Scale Hybrid Wind Solar Battery Based Microgrid. *IEEE Access* **2020**, *8*, 8336–8345. [[CrossRef](#)]
34. Zhou, L.; Zheng, Y.; Ouyang, M.; Lu, L. A study on parameter variation effects on battery packs for electric vehicles. *J. Power Sources* **2017**, *364*, 242–252. [[CrossRef](#)]
35. Alramlawi, M.; Li, P. Design Optimization of a Residential PV-Battery Microgrid with a Detailed Battery Lifetime Estimation Model. *IEEE Trans. Ind. Appl.* **2020**, *56*, 1. [[CrossRef](#)]
36. Lebron, C.; Andrade, F.; O’Neill, E.; Irizarry, A. An intelligent Battery management system for home Microgrids. In Proceedings of the IEEE 2016 IEEE Power & Energy Society Innovative Smart Grid Technologies Conference (ISGT), Minneapolis, MN, USA, 6–9 September 2016; pp. 1–5.
37. Davijani, H.K. Analysis and Control of a Microgrid with Converter Fed Distributed Energy Resources. Ph.D. Thesis, Tennessee Technological University, Cookeville, TN, USA, 2012.
38. Chandrakala Devi, S.; Singh, B.; Devassy, S. Modified generalised integrator-based control strategy for solar PV fed UPQC enabling power quality improvement. *IET Gen. Trans. Distrib.* **2020**, *14*, 3127–3138. [[CrossRef](#)]
39. Wang, Y.; Meng, J.; Zhang, X.; Xu, L. Control of PMSG-based wind turbines for system inertial response and power oscillation damping. *IEEE Trans. Sustain. Energy* **2015**, *6*, 565–574. [[CrossRef](#)]
40. Chen, H.; David, N. Analysis of permanent-magnet synchronous generator with Vienna rectifier for wind energy conversion system. *IEEE Trans. Sustain. Energy* **2013**, *4*, 154–163. [[CrossRef](#)]
41. Deghan, S.M.; Mohamadian, M.; Varjani, A.Y. A new variable-speed wind energy conversion system using permanent-magnet synchronous generator and Z-source inverter. *IEEE Trans. Energy Convers.* **2009**, *24*, 714–724. [[CrossRef](#)]
42. Chen, C.; Duan, S.; Cai, T.; Liu, B.; Hu, G. Smart energy management system for optimal microgrid economic operation. *IET Renew. Power Gener.* **2011**, *5*, 258–267. [[CrossRef](#)]
43. Bhende, C.N.; Mishra, S.; Malla, S.G. Permanent magnet synchronous generator based standalone wind energy supply system. *IEEE Trans. Sustain. Energy* **2011**, *2*, 361–373. [[CrossRef](#)]

44. Eltamaly, A.M.; Farh, H.M. Maximum power extraction from wind energy system based on fuzzy logic control. *Electr. Power Syst. Res.* **2013**, *97*, 144–150. [[CrossRef](#)]
45. Zhou, D.; Blaabjerg, F.; Franke, T.; Tnnes, M.; Lau, M. Comparison of wind power converter reliability with low-speed and medium-speed permanent-magnet synchronous generators. *IEEE Trans. Ind. Electron.* **2015**, *62*, 6575–6584. [[CrossRef](#)]
46. Polinder, H.; Ferreira, J.A.; Jensen, B.B.; Abrahamsen, A.B.; Atallah, K.; McMahon, R.A. Trends in wind turbine generator systems. *IEEE J. Emerg. Sel. Top. Power Electron.* **2013**, *1*, 174–185. [[CrossRef](#)]
47. Blaabjerg, F.; Ke, M. Future on Power Electronics for Wind Turbine Systems. *IEEE J. Emerg. Sel. Top. Power Electron.* **2013**, *1*, 139–152. [[CrossRef](#)]
48. Liu, J.; Miura, Y.; Bevrani, H.; Ise, T. Enhanced Virtual Synchronous Generator Control for Parallel Inverters in Micro grids Static Synchronous Generators for Distributed Generation and Renewable Energy. *IEEE Trans. Smart Grid* **2016**, *99*, 2268–2277.
49. Liu, J.; Miura, Y.; Ise, T. Comparison of Dynamic Characteristics Between Virtual Synchronous Generator and Droop Control in Inverter Based Distributed Generators. *IEEE Trans. Power Electron.* **2016**, *31*, 3600–3611. [[CrossRef](#)]
50. Bevrani, H.; Ghosh, A.; Ledwich, G. Renewable energy sources and frequency regulation: Survey and new perspectives. *IET Renew. Power Gener.* **2010**, *4*, 438–457. [[CrossRef](#)]
51. Diaz, G.A.; Gonzalez-Moran, C.; Gomez-Aleixandre, J.; Diez, A. Scheduling of droop coefficients for frequency and voltage regulation in isolated microgrids. *IEEE Trans. Power Syst.* **2010**, *25*, 489–496. [[CrossRef](#)]
52. Li, Y.; Xu, Z.; Xiong, L.; Song, G.; Zhang, J.; Qi, D.; Yang, H. A cascading power sharing control for microgrid embedded with wind and solar generation. *Renew. Energy* **2019**, *132*, 846–860. [[CrossRef](#)]
53. Meng, X.; Liu, J.; Liu, Z. A generalized droop control for gridsupporting inverter based on comparison between traditional droop control and virtual synchronous generator control. *IEEE Trans. Power Electron.* **2018**, *34*, 5416–5438. [[CrossRef](#)]
54. Wang, X.; Li, Y.W.; Blaabjerg, F.; Loh, P.C. Virtual-Impedance Based Control for Voltage-Source and Current-Source Converters. *IEEE Trans. Power Electron.* **2015**, *30*, 7019–7037. [[CrossRef](#)]
55. Muhamad, N.D.; Sahid, M.R.; Yatim, A.H.M.; Idris, N.R.N.; Ayob, N.S. Design of power stage and controller for DC-DC converter systems using PSPICE. In Proceedings of the International Conference on Power Electronics and Drives Systems, Kuala Lumpur, Malaysia, 28 October–1 November 2005; pp. 903–908.
56. Amandeep. ANFIS based control strategy for frequency regulation in AC microgrid. In Proceedings of the 2016 Fifth International Conference on Eco-Friendly Computing and Communication Systems (ICECCS), Bhopal, India, 8–9 December 2016; pp. 38–42.
57. Leonori, S.; Martino, A.; Rizzi, A.; Mascioli, F.M.F. Anfis synthesis by clustering for microgrids ems design. In Proceedings of the IJCCI 2017-9th International Joint Conference on Computational Intelligence, Funchal, Portugal, 1–3 November 2007; SciTePress: Setúbal, Portugal, 2017; pp. 328–337.